Available online at www.sciencedirect.com
SCIENCE DIRECT®
Polymer 44 (2003) 3347–3361
polymer
www.elsevier.com/locate/polymer

Effect of rubber particle size and rubber type on the mechanical properties of glass fiber reinforced, rubber-toughened nylon 6

D.M. Laura, H. Keskkula, J.W. Barlow, D.R. Paul*

Department of Chemical Engineering, Texas Materials Institute, University of Texas at Austin, Austin, TX 78712, USA

Received 20 February 2002; received in revised form 29 April 2002; accepted 1 May 2002

Abstract

The effects of rubber type and particle size on the mechanical properties of glass fiber reinforced blends of nylon 6 and EPR/EPR-*g*MA or SEBS/SEBS-*g*-MA were investigated; rubber particle size in the two systems could be controlled by varying the ratio of EPR to EPR-*g*-MA or SEBS to SEBS-*g*-MA. Unreinforced materials with the highest levels of toughness did not necessarily lead to the highest fracture energy when reinforced with 15 wt% glass fibers. Materials toughened with SEBS/SEBS-*g*MA, which are tougher in the absence of glass fibers had lower fracture energies when 15 wt% glass fibers are present. In general, smaller rubber particles led to higher fracture energies. Fracture analysis according to a modified essential work of fracture analysis reveals that SEBS/SEBS-*g*-MA have high values of the dissipative energy density, u_d, in the absence of glass fibers. When 15 wt% glass fibers are added, u_d is essentially zero for all the materials tested. The limiting specific fracture energy, u_0, on the other hand, was higher for both unreinforced and glass fiber reinforced EPR/EPR-*g*-MA toughened blends than for SEBS/SEBS-*g*-MA based materials. Transmission electron microscopy observations of fractured specimens indicate that glass fibers decrease the size of the damage zone of rubber toughened nylon 6. Shear yielding was seen in fractured specimens of reinforced nylon 6 blends containing either SEBS/SEBS-*g*-MA or EPR-*g*-MA, but the size of this shear yielded zone was larger for EPR/EPR-*g*-MA. In addition, EPR/EPR-*g*-MA based materials displayed craze-like deformations, while SEBS-*g*-MA materials did not exhibit this deformation process.

Keywords: Nylon 6; Glass fiber; Elastomer

1. Introduction

To generate rubber-toughened plastics with optimal mechanical properties, the rubber phase morphology and matrix–rubber particle interfacial properties must be controlled; the selection of an elastomer with appropriate mechanical properties is also critical to blend performance [1,2]. A rather extensive literature teaches how to control these variables to maximize toughness of such materials. Glass fibers are sometimes used in conjunction with rubber-toughening to produce materials with a balance of stiffness, strength, and toughness [3]; however, there is virtually no literature on how to optimize the dispersed rubber phase to achieve the best mechanical performance of glass fiber reinforced, rubber-toughened composites.

Both interfacial adhesion and rubber particle size can be controlled with the selection of appropriate compatibilization chemistry. For polyamide matrices, maleated elastomers are an effective route for obtaining good interfacial adhesion and controlling rubber particle size [4–9]. During melt processing, the maleic anhydride grafted to the elastomer of choice rapidly reacts with the amine end groups of the polyamide to give graft copolymers that simultaneously improve interfacial adhesion, reduce rubber particle size, and stabilize blend morphology. It is well established that there are upper and lower limits to the rubber particle size that produce super-tough pseudoductile thermoplastics [4–9]. These limits can be related to the toughening mechanisms associated with these materials. For instance, rubber particle cavitation is thought to change the stress state in the surrounding matrix initiating toughening mechanisms such as shear yielding and crazing [10,11]. Theoretical and experimental results indicate that rubber particle size is an important factor in cavitation; it is more difficult to initiate cavitation in smaller rubber

* Corresponding author. Tel.: +1-512-471-5392; fax: +1-512-471-0542.
E-mail address: drp@che.utexas.edu (D.R. Paul).

0032-3861/03/$ - see front matter © 2003 Elsevier Science Ltd. All rights reserved.
doi:10.1016/S0032-3861(03)00221-0

particles [10,12,13]. When rubber particles become too large without varying rubber content, the ligaments between the particles may be too large to yield [14,15]. Upper and lower limits on rubber particle size have been determined for a number of polymer blends [16], but it is unclear whether or not these same limits provide optimal mechanical properties when glass fibers are present.

The characteristics of the rubber are also important to blend performance. Rubber particle cavitation depends on the shear modulus of the rubber as well as the size of the particle [10]. Higher modulus rubbers require greater stresses during fracture in order to cavitate. If the stress required to cavitate the rubber particle is too high, the matrix may fail before cavitation occurs, and the toughening mechanisms initiated by cavitation do not have a chance to become operative. On the other hand, if the rubber cavitates too easily, the full potential of the matrix to absorb energy may not be realized [16].

This paper focuses on varying rubber particle size and rubber type with the goal of optimizing the mechanical properties of glass fiber reinforced, rubber-toughened nylon 6. A number of elastomers have been shown to produce super-tough blends when dispersed in a nylon 6 matrix. Two maleated elastomer systems that have proven quite effective for this purpose, i.e. those based on ethylene–propylene random copolymers (EPR) and styrene–hydrogenated butadiene–styrene triblock copolymers (SEBS), are used here. Control of rubber particle morphology is achieved by combining each rubber with its maleated counterpart (EPR-*g*-MA and SEBS-*g*-MA); similar results can be obtained by varying the amount of maleic anhydride grafted to the base elastomer [4,6–8].

2. Experimental

Table 1 provides details about the materials used in this study. The Kraton® materials are styrene–butadiene–styrene triblock copolymers where the butadiene block has been hydrogenated to produce a more thermally stable material. Both SEBS materials contain 29 wt% styrene. The ethylene–propylene rubbers (EPR) are random copolymers of ethylene and propylene containing 43 wt% ethylene. All of the elastomers and the nylon 6 are commercially available materials.

Glass fibers were in the form of a continuous roving comprised of 13 μm fibers with a proprietary surface treatment. In order to provide a known surface chemistry, these fibers were placed in a furnace at 500 °C for 30 min to remove the surface treatment supplied by the manufacturer. A silane coupling agent, 3-(triethoxysilyl)propylsuccinic anhydride, was applied to the surface of the glass fibers from a solution of 0.67 wt% anhydride silane coupling agent in a solution of ethanol with 10 wt% deionized water. The silane was allowed to react with the glass for 1 h. This surface treatment was shown to be an effective coupling agent for glass fibers used to reinforce rubber–toughened nylon 6 blends [17]. The glass fiber roving was coated with nylon 6 in a wire-coating, pultrusion type die and pelletized. This process produced very little wet-out of the glass fibers but was used to produce chopped glass, which was necessary for blending in the extrusion process.

All nylon 6 containing materials were dried in a vacuum oven for 24 h at 80 °C prior to any melt processing step. Blending was accomplished in a Killion single-screw extruder ($L/D = 30$, $D = 2.54$ cm), equipped with an intensive mixing head at 240 °C with a screw speed of 40 rpm. All materials were added simultaneously into the hopper of the extruder to give product of the desired compostion. Rubber content was determined on a glass fiber free basis such that reinforced and unreinforced materials can be compared properly. The total elastomer content of every material examined in this study is 20 wt% of the polymer mass.

The unmaleated EPR was received in bale form and required an additional processing step. The EPR bale was cut into cubes with sides of approximately 1 cm in length. These cubes were blended with equal parts of nylon 6 in a 250 ml Brabender internal mixer to form a 50/50 master batch. The master batch produced in the Brabender was in the form of large pieces that required grinding. Once ground, the master batch was dried and mixed with other materials for use in the melt blending process. The unmaleated SEBS and both maleated rubbers were received

Table 1
Materials used in this study

Material designation	Source	Manufacturer's designation	Description
Nylon 6	Allied signal	Capron B73WP	Nylon 6, $\bar{M}_n = 22,000$ End-group content: NH2 = 47.9 μequiv. g^{-1}, COOH = 43.0 μequiv. g^{-1}
Glass fiber	Owens-corning		13 μm E-glass roving treated with a proprietary sizing which was removed
EPR	Exxon chemical	Vistalon 457	Ethylene–propylene rubber 43 wt% ethylene, 53 wt% propylene
EPR-*g*-MA	Exxon chemical	Exxelor 1803	Ethylene–propylene rubber 43 wt% ethylene, 53 wt% propylene, 1.14 wt% grafted maleic anhydride
SEBS	Shell chemical	Kraton G 1652	Styrene–hydrogenated butadiene–styrene triblock copolymer 29 wt% styrene
SEBS-*g*-MA	Shell chemical	Kraton FG-1901X	Styrene–hydrogenated butadiene–styrene triblock copolymer 29 wt% styrene, 1.84 wt% grafted maleic anhydride

in a form suitable for extrusion, i.e. pellets, and did not require this additional processing.

Molding was performed in an Arburg Allrounder injection molding machine operating at an injection pressure of 70 bar and a holding pressure of 35 bar. Materials that did not contain any glass fibers were injection molded at 240 °C. Materials containing glass fibers required higher temperatures and were molded with the feed zone temperature set at 240 °C, then ramped up to 270 °C at the nozzle. The mold was held at 80 °C and the screw speed was maintained at 150 rpm for all materials. Izod bars, thickness = 6.35 or 3.18 mm and width = 12.7 mm, were molded for impact testing. ASTM D638 type I dogbone bars were molded for tensile testing which was performed on an Instron 1137 testing frame, upgraded for computerized data acquisition, at a rate of 5.08 mm/min. Standard notched Izod impact tests were performed on the 3.18 mm thick Izod bars according to ASTM D256. In addition, the 6.35 mm specimens were fractured in an instrumented Dynatup model 8200 drop tower in a three-point bend configuration. Testing was performed at 3.5 m/s with a falling mass of 14 kg. To avoid high levels of oscillation in the load response during instrumented impact tests, a rubber material was placed over the tup to dampen oscillations. Details of testing procedures and data analysis are given elsewhere [18–20]. Data from these tests were analyzed according to the model outlined by Mai and coworkers [21–29] which is based on Broberg's unified fracture theory [30,31]. The essential work of fracture, EWF, model is presented here in a slightly modified form because the specimen geometry and testing speed were different than those outlined by Mai. In this modified essential work of fracture model, the total energy used to fracture a specimen, U, per unit fracture surface area, A, is given by

$$\frac{U}{A} = u_0 + u_d \ell \tag{1}$$

where we call u_0 the limiting specific fracture energy and u_d the dissipative energy density. These parameters are considered phenomenological in nature and are not necessarily material parameters. The ligament length, ℓ, and other details of specimen geometry are shown in Fig. 1.

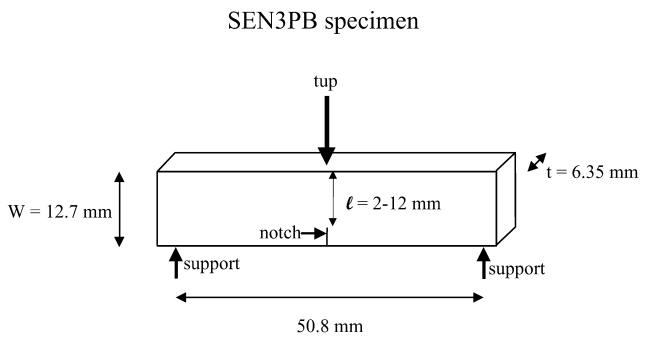

Fig. 1. Schematic representation of a single edge notched, three point bend (SEN3PB) specimen showing the ligament length (ℓ), specimen width (W), and specimen thickness (t).

In order to examine rubber phase morphology and toughening mechanisms, samples were imaged using a JEOL 200 CX transmission electron microscope. The samples were first cryogenically microtomed to 15 nm sections at −40 °C with a diamond knife. The sections were then stained using a 2% aqueous solution of phosphotungstic acid (PTA) for 30 min. Analysis of scanned TEM images was performed by Image, a computer program available from the National Institute of Health. The number average and weight average particle diameters were calculated according to the following formulas

$$\bar{d}_n = \frac{\Sigma n_i d_i}{\Sigma n_i} \tag{2}$$

$$\bar{d}_w = \frac{\Sigma n_i d_i^2}{\Sigma n_i d_i} \tag{3}$$

where n_i is the number of particles having diameter d_i. The polydispersity ratio is given by the ratio of $\bar{d}_w/\bar{d}_n$ and is regarded as a measure of the distribution of the dispersed phase particle size. A blend whose particles are all the same size would have a polydispersity ratio of 1; this ratio is greater than unity for all experimental blends.

Samples from Izod fracture tests were examined by transmission electron microscopy (TEM) to obtain insight about the operative toughening mechanisms. To prevent deformations during preparation of sections for TEM viewing, the Izod impact specimens were dipped into liquid nitrogen and then fractured at right angles to the fracture surface. A mesa cut was then made on the cryofractured surface such that the edge of the mesa cut was the fracture surface from the Izod impact test [32]. These samples were then cryogenically microtomed. Because it was difficult to produce a flat surface during this cryofracturing process, sections suitable for TEM observation were rarely produced in a single sectioning step; however, after the sections had been microtomed once there was a perfectly flat, polished surface on the specimen. This surface could then be mesa cut again to produce sections perpendicular to the Izod fracture surface that were not deformed in the sample preparation process.

3. Morphology development

Fig. 2 shows TEM photomicrographs from a series of nylon 6/EPR/EPR-*g*-MA blends reinforced with 15 wt% glass fibers where the nylon 6 phase has been stained dark with PTA. The total rubber mass (EPR + EPR-*g*-MA) makes up 20 wt% of the polymer mass (nylon 6 + EPR + EPR-*g*-MA) excluding the glass fibers. The total elastomer content for all blends in this study is 20 wt% of the polymer mass. Glass fiber content is based on the total mass of the material. This is an important distinction because comparisons between reinforced and unreinforced materials must be made on the proper basis. The EPR-*g*-MA content of the

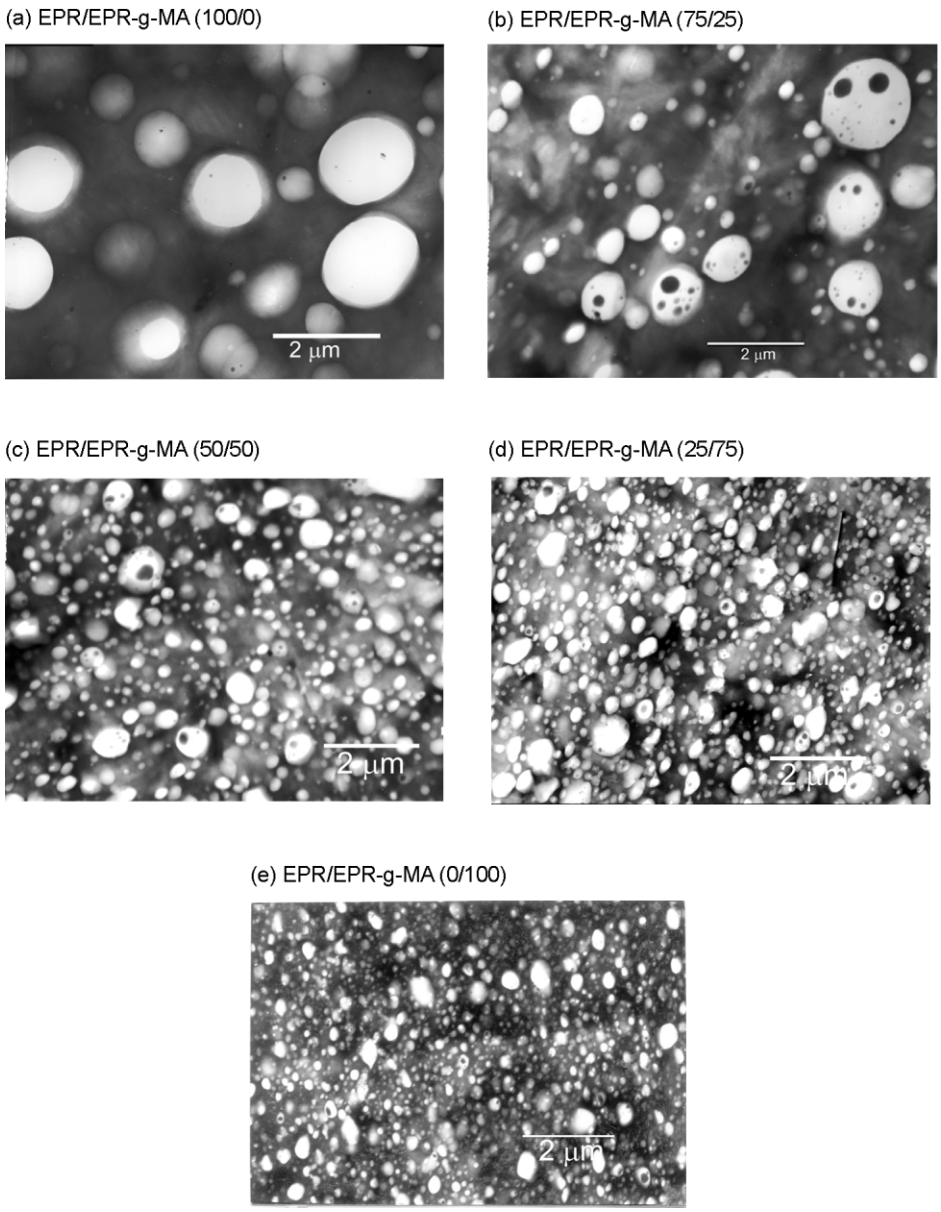

Fig. 2. TEM photomicrographs of nylon 6/EPR/EPR-*g*-MA blends reinforced with 15 wt% glass fibers containing EPR/EPR-*g*-MA in a ratio of (a) 100/0, (b) 75/25, (c) 50/50, (d) 25/75, and (e) 0/100. The total rubber mass (EPR + EPR-*g*-MA) makes up 20 wt% of the polymer mass (nylon 6 + EPR + EPR-*g*-MA) excluding the glass fibers.

rubber phase ranges from 0 to 100 wt% such that the maleic anhydride content of the rubber phase was varied between 0 and 1.14 wt%. The rubber particles shown here are somewhat irregular in shape and have nylon 6 occlusions. The rubber particles become smaller as the maleic anhydride content is increased. Similar observations have been made for this system where no glass fibers are present [7,8].

Fig. 3 shows the quantitative results of image analysis of these specimens. In Fig. 3(a), the weight average rubber particle size is plotted versus the maleic anhydride content in the EPR phase. As maleic anhydride content is increased from 0 to 1.14 wt%, the rubber particle size decreases from about 1 to about 0.2 μm; a similar trend was reported earlier for the case without glass fibers [7,8].

The glass fiber reinforced materials have smaller rubber particles than the unreinforced materials. Oshinski and coworkers have examined the effect of nylon 6 molecular weight on the size of rubber particles generated in a similar blending process (without glass fibers) [7,8]. It was found that the rubber particles become smaller as the nylon 6 molecular weight was increased; this trend was attributed to the corresponding increase in melt viscosity. Adding glass fibers also increases the apparent viscosity of the polymer melt. Oshinski et al. found the EPR-*g*-MA particle size to be 0.23 μm in a nylon 6 matrix with $\bar{M}_n = 22,000$ and Brabender torque (a measure of melt viscosity) of 6.6 N m and 0.15 μm for a matrix with $\bar{M}_n = 29,300$ and Brabender torque of 14.1 N m. In the present case, addition of glass

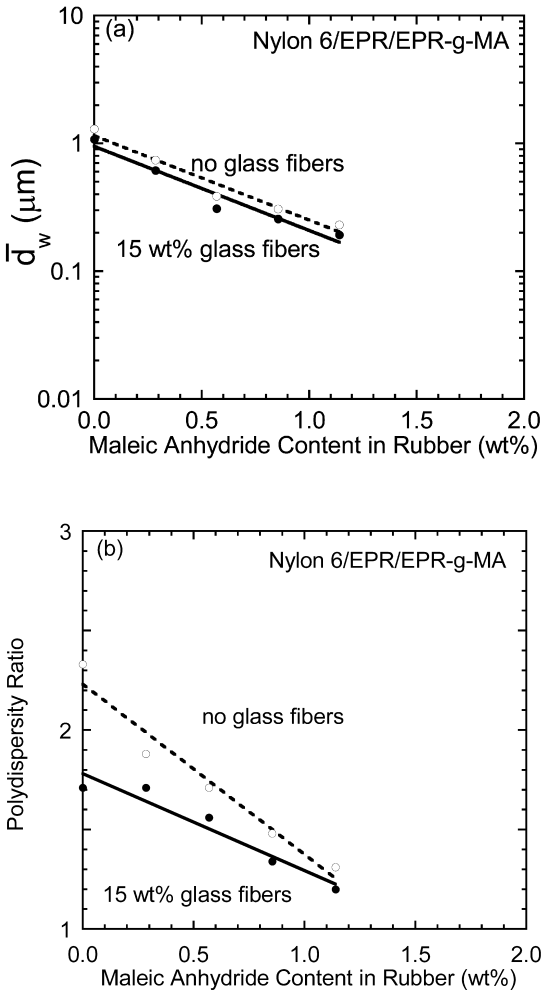

Fig. 3. Rubber particle size analysis for nylon 6/EPR/EPR-*g*-MA blends where (a) weight average rubber particle diameter ($\bar{d}_w$) and (b) polydispersity ratio ($\bar{d}_w/\bar{d}_n$) are plotted versus maleic anhydride content in the rubber phase. The total rubber mass (EPR + EPR-*g*-MA) makes up 20 wt% of the polymer mass (nylon 6 + EPR + EPR-*g*-MA) excluding the glass fibers.

fibers increases the Brabender torque from 6.6 to 9.5 N m (at 15 wt% glass fibers), while the rubber particle size decreased from 0.23 to 0.19 μm. The decrease in rubber particle size caused by addition of glass fibers is approximately the same as that caused by increasing the matrix molecular weight to give a corresponding change in viscosity.

Fig. 3(b) shows the polydispersity ratio plotted versus maleic anhydride content in the rubber phase. As maleic anhydride content is increased, the polydispersity ratio decreases. In addition, the polydispersity is lower for blends containing glass fibers. Oshinski and coworkers found the same trend in polydispersity ratio versus maleic anhydride content [7,8]; it was also found that increasing the nylon 6 molecular weight lowered the polydispersity ratio. Thus, the particle size distribution seems to become more narrow as matrix melt viscosity increases by either increasing molecular weight or by adding glass fibers.

Fig. 4 shows TEM photomicrographs for a series of glass fiber reinforced nylon 6/SEBS/SEBS-*g*-MA blends containing from 0 to 100 wt% SEBS-*g*-MA in the rubber phase. The total mass of the elastomer is 20 wt% of the polymer mass. The nylon 6 phase is stained dark with PTA. Like the nylon 6/EPR blends described above, the rubber particles become smaller as the maleic anhydride content increases. The rubber particles in parts (a) and (b) have considerably more occluded nylon 6 particles than those in parts (c)–(e) where there is more maleic anhydride present. At high maleic anhydride contents, the rubber particle size approaches the thickness of the microtomed section which causes poor image quality.

The results of analysis of these images are shown in Fig. 5. For the material containing 15 wt% glass fibers, the weight average rubber particle diameter decreases from about 0.6 to 0.05 μm. The blends based on SEBS rubber have a lower average particle diameter and lower polydispersity ratios when glass fibers are present, just as observed for blends based on EPR rubber. At the same maleic anhydride content, materials made with SEBS have a smaller rubber particle diameter than do materials made with EPR; the same trend was observed by Oshinski et al. [6–8].

4. Mechanical properties

The mechanical properties of these materials measured in tensile tests are summarized in Table 2. Since the tensile properties do not depend on rubber particle size, the properties for only one of each of these elastomers are given here. The SEBS elastomer has a higher tensile strength and modulus than EPR which probably accounts for the higher values for yield strength and modulus for blends containing SEBS. For blends based on either elastomer system, addition of 15 wt% glass fibers more than offsets the loss of modulus and yield strength caused by the addition of rubber to the polyamide.

Fig. 6 shows the room temperature notched Izod impact strength of nylon 6/EPR/EPR-*g*-MA plotted versus weight average rubber particle diameter (part a) and maleic anhydride content in the rubber (part b). When no glass fibers are present, there is a maximum in fracture energy at a weight average particle size between 0.3 and 0.4 μm. For materials containing 15 wt% glass fibers, there is no maximum; instead the fracture energy steadily increases as the rubber particle size becomes smaller. The glass fiber reinforced materials do not follow the same qualitative trend as the unreinforced materials, and there seems to be no correlation between the toughness of the unreinforced materials and those containing 15 wt% glass fibers.

The relationships between notched Izod impact strength for nylon 6/SEBS/SEBS-*g*-MA blends and the weight average particle diameter or maleic anhydride content are shown in Fig. 7. When no glass fibers are present, there is a

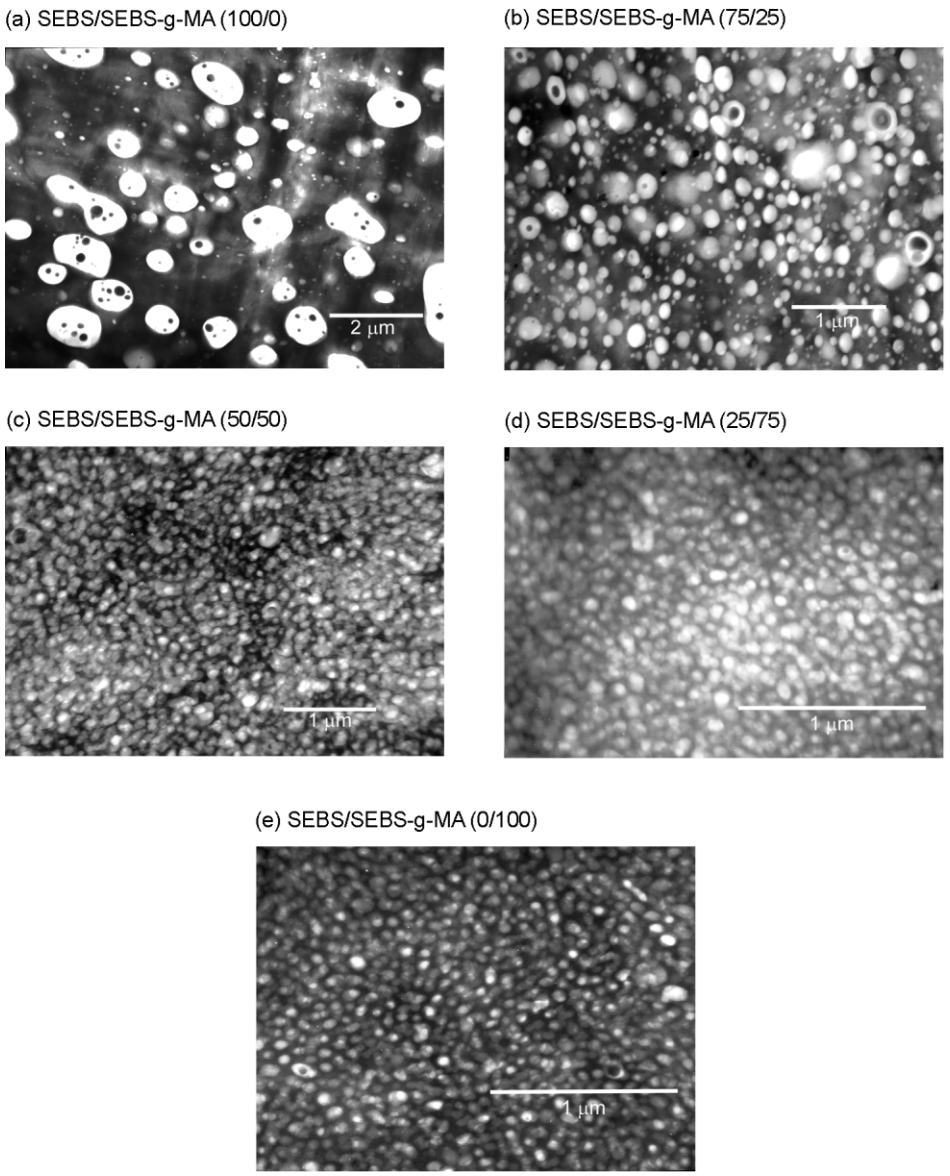

Fig. 4. TEM photomicrographs of nylon 6/SEBS/SEBS-*g*-MA blends reinforced with 15 wt% glass fibers containing SEBS/SEBS -*g*-MA in a ratio of (a) 100/0, (b) 75/25, (c) 50/50, (d) 25/75, and (e) 0/100. The total rubber mass (SEBS + SEBS -*g*-MA) makes up 20 wt% of the polymer mass (nylon 6 + SEBS + SEBS -*g*-MA) excluding the glass fibers.

strong maximum in toughness when the rubber phase contains SEBS/SEBS-*g*-MA in a (25/75) ratio as reported by Oshinski et al. [6,7]. This material has a weight average particle diameter of 0.33 μm, which is in the same range of the maximum toughness for materials made with EPR/EPR-*g*-MA mixtures. The maximum notched Izod impact value of 950 J/m is much higher than any material made with EPR/EPR-*g*-MA mixtures; however, when 15 wt% glass fiber is added, the SEBS/SEBS-*g*-MA toughened materials have a lower fracture energy than the EPR/EPR-*g*-MA based materials of the same particle size. Unlike the glass fiber reinforced EPR/EPR-*g*-MA toughened materials,

Table 2
Tensile properties of nylon 6/elastomer (80/20) blends

Glass fiber content (wt%)	EPR-*g*-MA		SEBS-*g*-MA	
	Tensile modulus (GPa)	Yield strength (MPa)	Tensile modulus (GPa)	Yield strength (MPa)
0	1.8	47	2	51
15	4.0	80	4.1	83
Neat nylon	2.8	70		

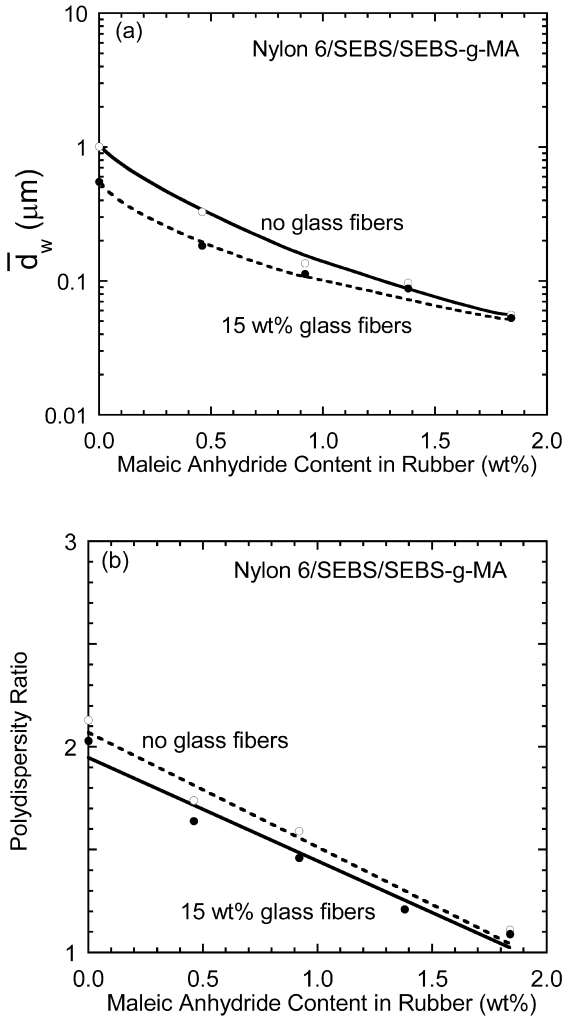

Fig. 5. Rubber particle size analysis for nylon 6/SEBS/ SEBS -*g*-MA blends where (a) weight average rubber particle diameter ($\bar{d}_w$) and (b) polydispersity ratio ($\bar{d}_w/\bar{d}_n$) are plotted versus maleic anhydride content in the rubber phase. The total rubber mass (SEBS + SEBS-*g*-MA) makes up 20 wt% of the polymer mass (nylon 6 + SEBS + SEBS-*g*-MA) excluding the glass fibers.

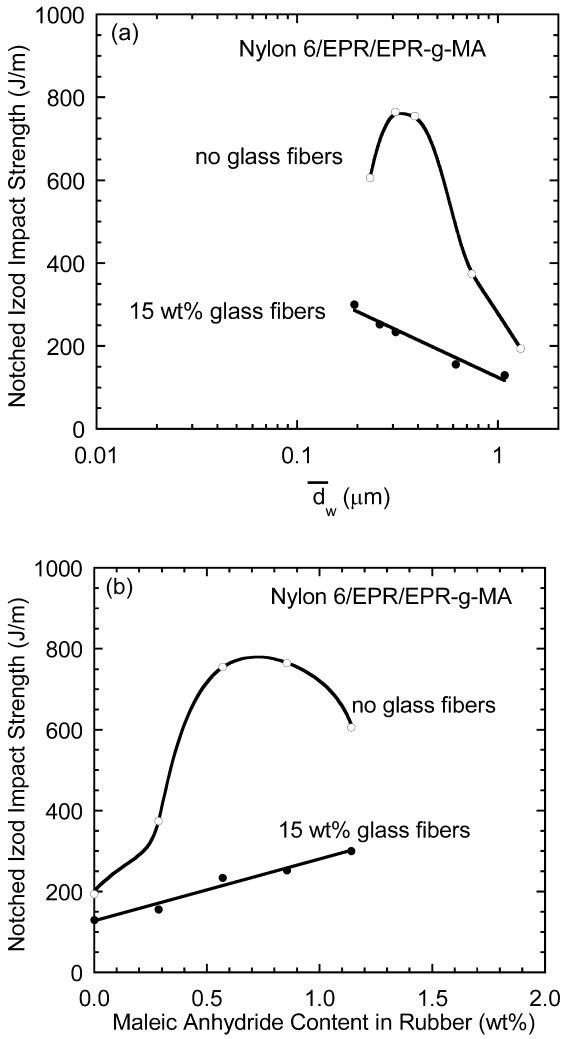

Fig. 6. Notched Izod impact strength for blends of nylon 6/EPR/EPR-*g*-MA as a function of (a) weight average rubber particle diameter ($\bar{d}_w$) and (b) maleic anhydride content in the rubber phase. The total rubber mass (EPR + EPR-*g*-MA) makes up 20 wt% of the polymer mass (nylon 6 + EPR + EPR-*g*-MA) excluding the glass fibers.

where fracture energy continually increased as the rubber particles became smaller, the glass fiber reinforced SEBS/ SEBS-*g*-MA toughened materials have a relatively constant value of notched Izod impact strength for compositions that contain maleated rubber. The unmaleated rubber has a coarse morphology and poor adhesion with the polyamide matrix and is expected to have a lower impact energy.

5. Dynatup fracture tests

The above results reveal that nylon 6/SEBS/SEBS-*g*-MA blends are tougher than EPR/EPR-*g*-MA based materials when no glass fibers are present but have lower values of toughness when 15 wt% glass fibers are present. The relatively simple notched Izod impact test does not provide insights into the reasons behind this behavior; however, a more detailed fracture analysis may help to explain the differences in the performance of these systems. Fig. 8 shows force–displacement diagrams for unreinforced nylon 6/EPR/EPR-*g*-MA blends where the rubber phase is 20 wt% of the polymer mass. The material containing no maleated rubber fails at a substantially lower load and displacement than corresponding materials containing maleation. The material containing 75 wt% maleated rubber reaches higher loads than does the material with 100 wt% EPR-*g*-MA. Although this difference is small, it persists throughout the fracture process, resulting in a significantly higher total fracture energy. The fracture behavior changes considerably when these materials contain 15 wt% glass fibers as shown in Fig. 9. All glass fiber reinforced materials reach higher loads than do their unreinforced counterparts. The material containing no maleated rubber is brittle and fails at a lower load than the materials that contain EPR-*g*-MA. Unlike the case without glass fibers, the reinforced material based on

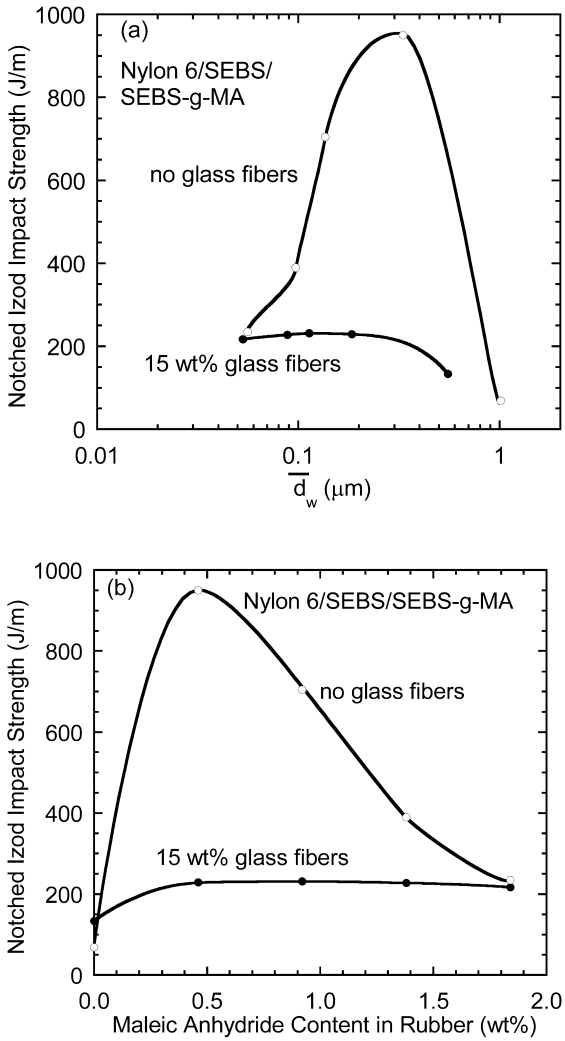

Fig. 7. Notched Izod impact strength for blends of nylon 6/SEBS/SEBS-*g*-MA as a function of (a) weight average rubber particle diameter ($\bar{d}_w$) and (b) maleic anhydride content in the rubber phase. The total rubber mass (SEBS + SEBS-*g*-MA) makes up 20 wt% of the polymer mass (nylon 6 + SEBS + SEBS-*g*-MA) excluding the glass fibers.

100 wt% EPR-*g*-MA reaches a higher load than does the material with 75 wt% EPR-*g*-MA.

The total fracture energy per unit area for the unreinforced nylon 6/EPR/EPR-*g*-MA blends is plotted versus ligament length in Fig. 10; again the total rubber mass is 20 wt% of the polymer mass. The lines drawn represent the best fit of the data to Eq. (1). When no maleated rubber is present, the specimens fail in a brittle manner. Linear elastic fracture mechanics (LEFM) provides a more appropriate model for brittle materials than the EWF model discussed above. According to the LEFM model [33], the energy to fracture a specimen, U, is given by

$$U = G_{Ic} t W \phi + U_k \tag{4}$$

where G_{Ic} is the critical strain energy release rate and U_k is the kinetic energy of the specimen after fracture. The specimen thickness, t, and width, W, are shown in Fig. 1.

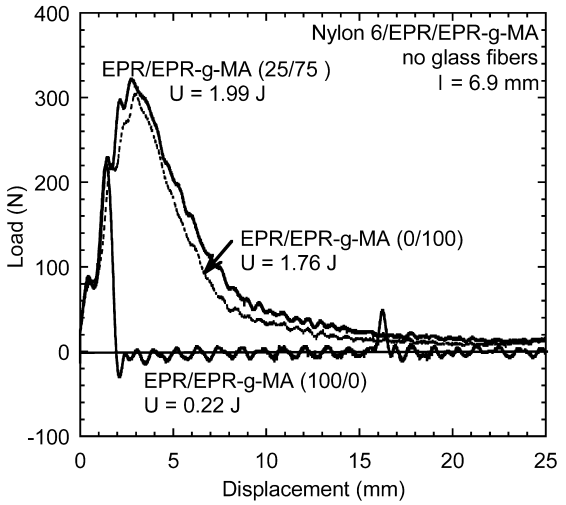

Fig. 8. Force versus displacement for unreinforced nylon 6/EPR/EPR-*g*-MA blends of the same ligament length (ℓ). The total rubber mass makes up 20 wt% of the polymer mass.

The parameter ϕ describes the relationship between specimen compliance, C, and crack length, a, and is defined as

$$\phi = \frac{C}{\mathrm{d}C/\mathrm{d}(a/W)} \tag{5}$$

The relationship between U/A and ℓ for a brittle material can be determined from the LEFM model represented in Eq. (4) by dividing by fracture surface area, A ($= \ell t$), to give

$$\frac{U}{A} = G_{Ic} W \left(\frac{\phi}{\ell}\right) + \frac{U_k}{\ell t} \tag{6}$$

This result is useful for understanding the shape of fracture energy data for brittle materials that follow the LEFM model when plotted in the form of Fig. 10, i.e. U/A versus ℓ. In Eq. (6), as the crack length approaches zero (ℓ approaches W), ϕ becomes large in value such that the

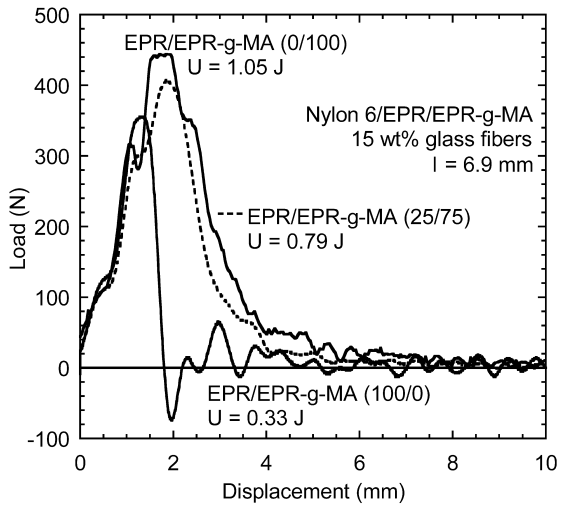

Fig. 9. Force versus displacement for nylon 6/EPR/EPR-*g*-MA blends reinforced with 15 wt% glass fibers of the same ligament length (ℓ). The total rubber mass makes up 20 wt% of the polymer mass, excluding the glass fibers.

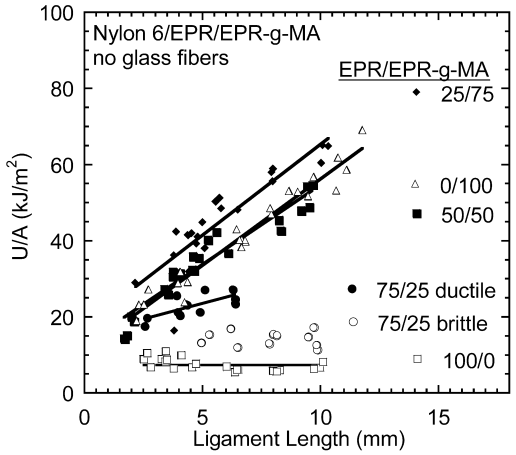

Fig. 10. Fracture energy per unit area (U/A) versus ligament length for unreinforced nylon 6/EPR/EPR-*g*-MA blends. The total rubber mass makes up 20 wt% of the polymer mass.

first term on the right hand side of this equation becomes very large for long ligament lengths. The second term always decreases with increasing ligament length. The net result is that for a brittle material the fracture energy per unit area is concave upwards rather than linear when plotted against ligament length. This results in negative slopes when such data are analyzed according to Eq. (1). This behavior has been described in more detail in earlier papers [18,19]. According to the EWF analysis, the slopes of plots of U/A versus ℓ are regarded as a measure of energy absorbing processes that occur away from the fracture surface, i.e. the non-essential work of fracture in the plastic process zone. For the purposes of this paper, it will be assumed that in brittle materials these processes absorb a negligible amount of energy; thus, the slopes of U/A versus ℓ plots are forced to zero for all brittle materials.

Brittle materials exhibit qualitatively different characteristics in fracture tests than ductile materials. Typically, the load for a brittle specimen in a fracture test will increase to a maximum value and drop off very sharply thereafter, as seen in load displacement diagrams such as Fig. 8. The load signal, measured by the load cell, often registers below zero after the specimen snaps. In this study, this behavior is observed for all of the materials that do not contain any maleated rubber. In addition the nylon 6/EPR/EPR-*g*-MA (80/15/5) blend reinforced with 15 wt% glass fibers also fractured in this manner. When ductile materials are fractured, on the other hand, the load reaches a maximum value and trails off more gradually thereafter. Every material tested in this study, other than the brittle materials mentioned above, exhibited some level of ductility. For the unreinforced ductile materials, the load decreases quite slowly after maximum load is reached. When 15 wt% glass fibers are present, the load tapers off more rapidly but the decrease in load is more gradual than observed for the materials classified as brittle. When fracture energy per unit area is plotted against ligament length, ductile materials generally form plots that have straight lines with positive slopes. When glass fibers are present, the slopes of these lines, which is the dissipative energy density u_d, may be nearly zero; however, this does not mean that the materials fail in a brittle manner. For brittle materials, plots of fracture energy per unit area versus ligament length are generally concave upwards for reasons discussed above, and do not form straight lines. Only the materials classified above as brittle exhibit this curvature in such plots.

In the Dynatup fracture tests of unreinforced nylon 6/EPR/EPR-*g*-MA blends, the material that contains EPR/EPR-*g*-MA in a 25/75 ratio has the highest fracture energy. This material also has the highest fracture energy in the notched Izod impact strength test. The materials containing 100 wt% EPR-*g*-MA and 50/50 EPR/EPR-*g*-MA behave nearly identical in this test; however, the material with 50 wt% EPR-*g*-MA had a much higher fracture energy in the Izod impact test. The conditions used in the Dynatup test involve sharper notches and thicker specimens than the Izod test. The former testing conditions are more severe than the latter, and the range of optimal particle size is not necessarily the same. This may account for the fact that the material with 50 wt% EPR-*g*-MA does not outperform the material with 100 wt% EPR-*g*-MA in the Dynatup test. The material containing a 75/25 EPR/EPR-*g*-MA mixture undergoes a ductile-to-brittle transition with respect to ligament length. Such behavior has been described in detail in prior papers [19,20,34].

Fig. 11 shows the Dynatup results for nylon 6/EPR/EPR-*g*-MA blends reinforced with 15 wt% glass fibers. The materials containing 0 and 25 wt% EPR-*g*-MA are brittle; thus, the slopes of the lines for these materials have been forced to zero for reasons discussed above. The fracture energies of the remaining materials follow the same order as the fracture energies from the Izod tests. There does not seem to be any correlation between the fracture energy of the unreinforced materials from Fig. 10 and their glass fiber reinforced counterparts in Fig. 11.

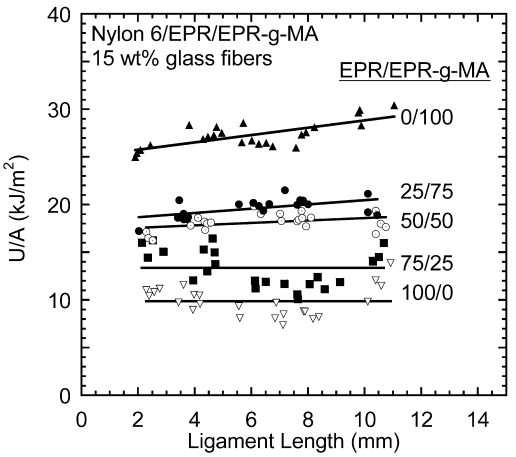

Fig. 11. Fracture energy per unit area (U/A) versus ligament length for nylon 6/EPR/EPR-*g*-MA blends reinforced with 15 wt% glass fibers. The total rubber mass makes up 20 wt% of the polymer mass, excluding the glass fibers.

Fig. 12 shows force–displacement diagrams for some unreinforced nylon 6/SEBS/SEBS-*g*-MA blends where the total rubber mass (SEBS + SEBS-*g*-MA) makes up 20 wt% of the polymer mass. The material containing 100 wt% SEBS-*g*-MA does not reach as high a load or displacement as the other materials that contain maleated rubber. Other studies have attributed this lack of toughness to the fact that the particle size for this material is below the lower limit for effective toughening [6,7]. The material based on 25/75 SEBS/SEBS-*g*-MA, which was the toughest of Izod results, also has the highest fracture energy in the Dynatup impact tests. This high level of toughness seems to be a result of the fact that this material reaches a higher load during the fracture tests. The SEBS/SEBS-*g*-MA based materials containing 25, 50, and 75 wt% SEBS-*g*-MA all reach higher loads during impact tests than the EPR/EPR-*g*-MA based materials. The higher loads are reached without any loss in ductility, the result being higher fracture energies.

Fig. 13 shows examples of load–displacement diagrams for two materials based on 25 and 50 wt% SEBS-*g*-MA that are reinforced with 15 wt% glass fibers. In the absence of glass fibers, the material with 25 wt% SEBS-*g*-MA reaches higher loads during fracture and has a much higher total fracture energy; however, when glass fibers are added there is no discernible difference between the fracture response of the two materials. Fig. 14 compares load–displacement diagrams for composites toughened with SEBS/SEBS-*g*-MA and with EPR/EPR-*g*-MA where the two materials have nearly the same rubber particle size. The main difference between the two is that the load for the EPR/EPR-*g*-MA toughened material does not decline quite as rapidly after the maximum load is reached; this results in a higher fracture energy.

The total fracture energy per unit area for the unreinforced SEBS/SEBS-*g*-MA based materials is plotted versus ligament length in Fig. 15. The material containing

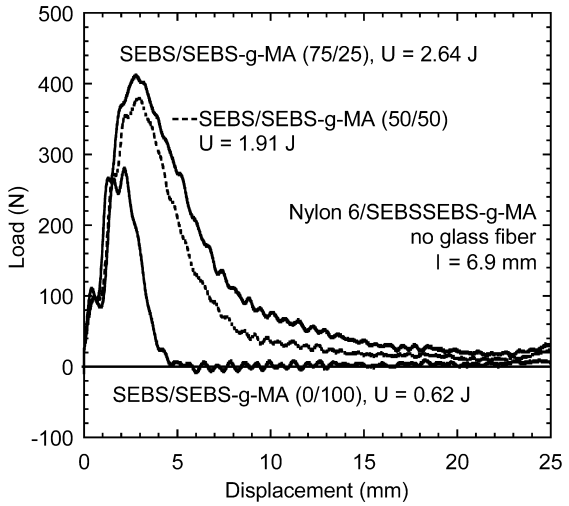

Fig. 12. Force versus displacement for unreinforced nylon 6/SEBS/SEBS-*g*-MA blends of the same ligament length (ℓ). The total rubber mass makes up 20 wt% of the polymer mass.

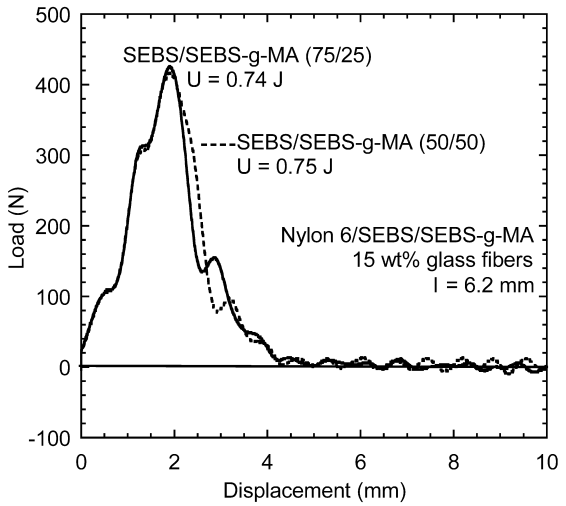

Fig. 13. Force versus displacement for nylon 6/SEBS/SEBS-*g*-MA blends reinforced with 15 wt% glass fibers of the same ligament length (ℓ). The total rubber mass makes up 20 wt% of the polymer mass, excluding the glass fibers.

25 wt% SEBS-*g*-MA has an exceptionally large slope or dissipative energy density, u_d; this term rather than u_0 gives rise to the high level of toughness for this material. The slope is associated with fracture processes that occur in an outer plastic zone away from the fracture surface, but the component of fracture energy that results from processes in the outer plastic zone is not likely to be significant when glass fibers are present because of the mechanical confinement imposed on the polymer matrix by the glass fibers. This effect can be seen in Fig. 16 where all the reinforced materials have essentially zero slope or a dissipative energy density near zero.

Fig. 17 shows the limiting specific fracture energy, u_0, plotted versus rubber particle size for blends of nylon 6

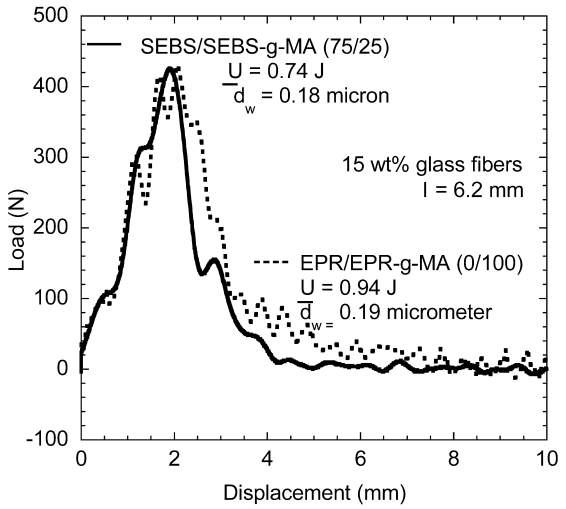

Fig. 14. Force versus displacement for a nylon 6/EPR/EPR-*g*-MA blend and a nylon 6/SEBS/SEBS-*g*-MA blend reinforced with 15 wt% glass fibers of the same ligament length (ℓ) and weight average rubber particle diameter ($\bar{d}_w$). The total rubber mass makes up 20 wt% of the polymer mass, excluding the glass fibers.

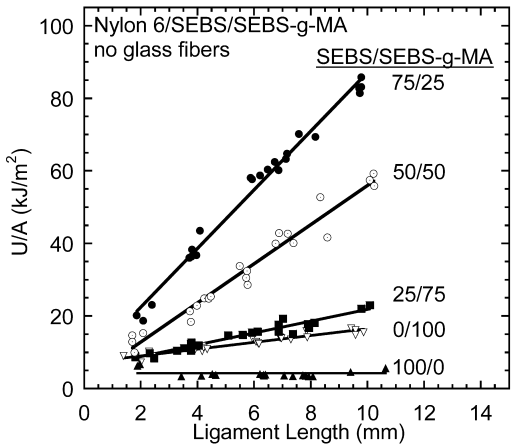

Fig. 15. Fracture energy per unit area (U/A) versus ligament length for unreinforced nylon 6/SEBS/SEBS-g-MA blends. The total rubber mass makes up 20 wt% of the polymer mass.

toughened with EPR/EPR-g-MA and SEBS/SEBS-g-MA at 20 wt% elastomer in the polymer phase. Data for unreinforced materials are shown in part (a); part (b) shows data for the corresponding materials with 15 wt% glass fibers. In part (a), it is difficult to tell if there is any relationship between rubber particle size and u_0 because of the scatter in the data; however, the unreinforced SEBS/SEBS-g-MA based materials have lower values of u_0 than the ERP/EPR-g-MA based materials at the same weight average particle diameter. The specific limiting fracture energy of all of the materials in part (a) is increased when 15 wt% glass fibers are added, as seen in part (b). The presence of glass fibers does not change the relative values of u_0; the EPR/EPR-g-MA toughened materials still have higher values of u_0 than SEBS/SEBS-g-MA based materials. The value of u_0 is increased for EPR/EPR-g-MA toughened materials when rubber particles become smaller; however, the SEBS/SEBS-g-MA materials have a more constant value of u_0 when the maleated rubber content is above zero. The limiting specific

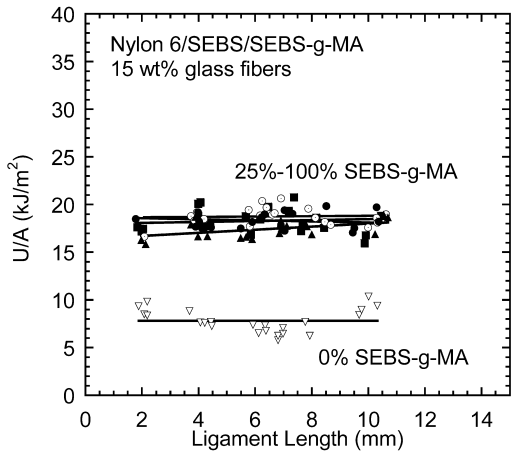

Fig. 16. Fracture energy per unit area (U/A) versus ligament length for nylon 6/SEBS/SEBS-g-MA blends reinforced with 15 wt% glass fibers. The total rubber mass makes up 20 wt% of the polymer mass, excluding the glass fibers.

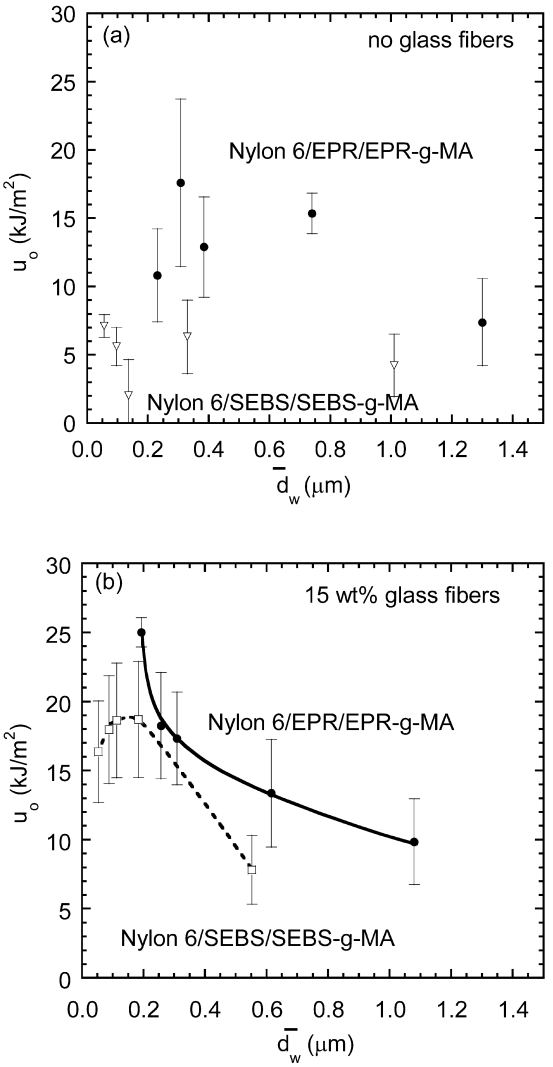

Fig. 17. Limiting specific fracture energy (u_0) versus weight average rubber particle diameter ($\bar{d}_w$) for nylon 6/EPR/EPR-g-MA and nylon 6/SEBS/-SEBS-g-MA blends that are (a) unreinforced and (b) reinforced with 15 wt% glass fibers. The total rubber mass makes up 20 wt% of the polymer mass, excluding the glass fibers.

fracture energy is lower for the material SEBS based material that contains no maleated rubber where rubber particle size is large. Fig. 18 shows plots of the dissipative energy density, u_d, analogous to the plots of u_0 in Fig. 17. The dissipative energy density of the unreinforced materials follows the same trend as a function of rubber particle size as the notched Izod impact strength; there is a maximum in u_d between 0.3 and 0.4 μm. The unreinforced SEBS/SEBS-g-MA toughened materials have higher values of u_d than the unreinforced EPR/EPR-g-MA based materials of the same weight average particle diameter; however, addition of 15 wt% glass fibers reduces the dissipative energy density to nearly zero for all materials. According to the EWF model, the parameter u_d is associated with energy absorbing processes, e.g. shear yielding, that occur in an outer plastic zone away from the fracture surface. It has been demonstrated that the incorporation of glass fibers into rubber

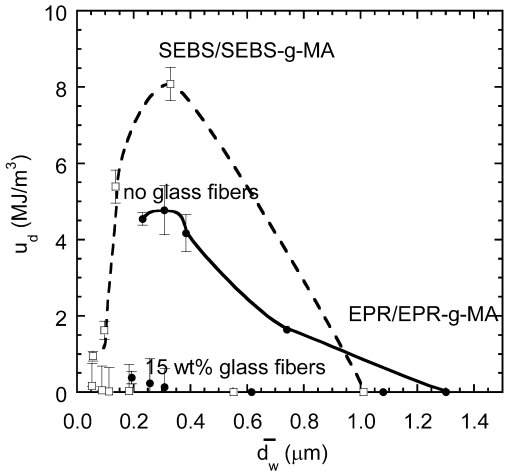

Fig. 18. Dissipative energy density (u_d) versus weight average rubber particle diameter ($\bar{d}_w$) for nylon 6/EPR/EPR-*g*-MA and nylon 6/SEBS/-SEBS-*g*-MA blends. The total rubber mass makes up 20 wt% of the polymer mass, excluding the glass fibers.

toughened polymers prevents any large-scale deformations away from the fracture surface because of the constraints imposed upon the matrix by the glass fibers; thus, it is reasonable that u_d should be near zero for glass fiber containing materials [18].

The data in Figs. 6 and 7 show that unreinforced nylon 6/SEBS/SEBS-*g*-MA blends have higher Izod impact energies than nylon 6/EPR/EPR-*g*-MA blends with the same rubber particle size. The values for notched Izod impact strength follow the same trend as u_d; however, this parameter is decreased to nearly zero by the addition of 15 wt% glass fibers. The limiting specific fracture energy, on the other hand, is larger for EPR/EPR-*g*-MA based materials and is increased by the presence of glass fibers. The notched Izod impact test, which is particularly sensitive to changes in u_d, is a relatively simple, single point test that is incapable of separating these two fracture components. For the materials used in this study, the fracture energies of the unreinforced materials from the Izod test is a poor predictor of the relative fracture energies when glass fibers are added; the limiting specific fracture energy of the unreinforced blends is a better predictor. This could be a helpful guide for selecting the rubber type when designing glass fiber reinforced rubber toughened materials.

6. Deformation mechanisms

Fig. 19 shows a TEM photomicrograph from a fractured Izod specimen of a blend toughened with 50/50 EPR/EPR-*g*-MA and reinforced with 15 wt% glass fibers. The left side of this image shows the fracture surface generated in an Izod test. A zone of shear yielded material extends more than 10 μm from the fracture surface. Measurements from fractured EPR/EPR-*g*-MA toughened specimens reinforced with 15 wt% glass fibers reveal a deformed zone that is

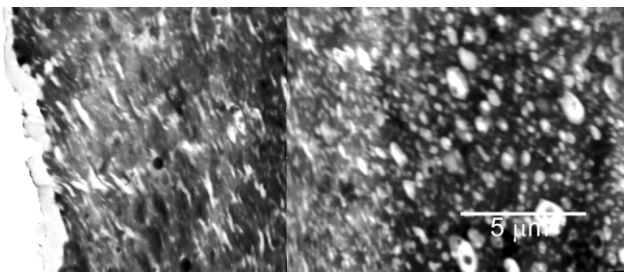

Fig. 19. TEM photomicrograph from a fractured Izod specimen of a blend toughened with 50/50 EPR/EPR-*g*-MA and reinforced with 15 wt% glass fibers. The left-hand side of the image shows the fracture surface. The total rubber mass makes up 20 wt% of the polymer mass, excluding the glass fibers.

approximately the same size for all of the materials regardless of the amount of maleated rubber used except, of course, in the limit of no maleated rubber. In the latter case, the particle size is too large for effective toughening and extensive shear yielding even in the unreinforced material. On the other hand, unreinforced 80/20 blends of nylon 6 with EPR-*g*-MA have a shear deformed zone extending about 50 μm from the fracture surface [13]. The reduced size of the deformed zone when glass fibers are present is consistent with the low values of the dissipative energy density, u_d, and the physical interpretation of this quantity.

Fig. 20 shows a TEM photomicrograph of a fractured specimen from a blend toughened with 100 wt% EPR-*g*-MA blend and reinforced with 15 wt% glass fibers. This specimen shows an interesting feature emanating from the fracture surface. Like a craze, there are a series of voids that appear to be stabilized by parallel polyamide ligaments; however, there are some significant differences between this feature and traditional crazes. Although shear yielding is thought to be the dominant deformation mechanism in rubber-toughened polyamides, crazing has been documented in some instances for polyamide systems [35,36]. This structure is larger (approximately 1 μm thick at its base) than other crazes seen in polyamides. In addition, crazes typically have more fibrils with interconnected voids over a given length than the relatively few ligaments seen in Fig. 20 [37]. Fig. 21 shows another such feature for a material similar to that shown in Fig. 20. In this case, there is clear evidence of cavitation in the rubber particles. Typically, crazes are initiated in rubber toughened materials by large rubber particles at equatorial sites where stress concentration is the highest, sometimes subsequent to rubber particle cavitation [37]. In this instance, there is a row of cavitated rubber particles with what appears to be yielded polyamide ligaments between them. Thus, the rubber particles are located within this deformation zone rather than at the point of origin. Other investigators have reported regions of deformation similar to those seen in Figs. 20 and 21. Lazerri and Bucknall showed that fractured specimens of rubber toughened polyamides had lines of cavitated rubber particles separated by shear yielded nylon 6

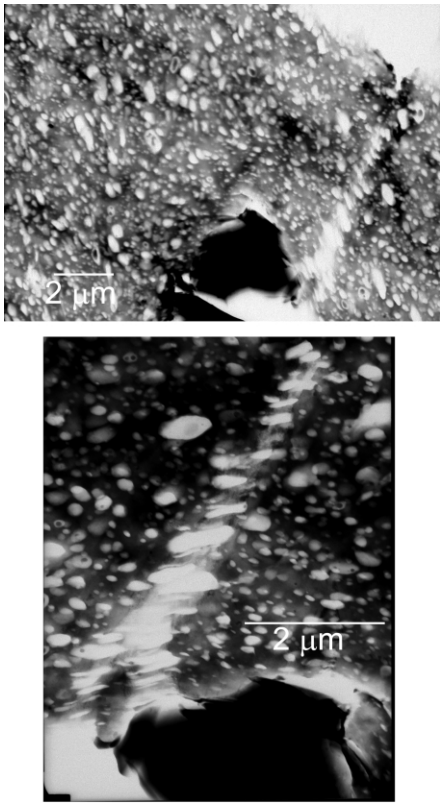

Fig. 20. TEM photomicrograph from a fractured Izod specimen of a blend toughened with 100 wt% EPR-*g*-MA and reinforced with 15 wt% glass fibers showing a dilational band originating at the glass fiber. The total rubber mass makes up 20 wt% of the polymer mass, excluding the glass fibers.

ligaments and referred to these features as 'dilational bands' [13,38]. Sue et al. saw similar linear arrays of cavitated rubber particles in rubber toughened epoxy matrices and called them 'croids' [39–41].

The deformation feature seen in Fig. 21 seems to be associated with rubber particles that are on the high end of the particle size distribution. This may be due to the fact that larger particles cavitate more easily than the smaller particles within the inevitable distribution of sizes [10]. However, it would be incorrect to conclude that larger rubber particles are desirable for glass fiber reinforced materials since this study has shown that smaller rubber particles lead to higher fracture energies. At fixed rubber concentration, large rubber particles lead to large interparticle distances, and, unfortunately, smaller interparticle distances are needed to facilitate matrix yielding [14,15].

The glass fiber reinforced material toughened with 100 wt% EPR-*g*-MA has a higher fracture energy than the other reinforced EPR/EPR-*g*-MA based materials; however, the shear yielded zone is the same for all four materials that have EPR-*g*-MA contents above zero. Comparisons of fractured nylon 6/EPR/EPR-*g*-MA specimens that are reinforced with 15 wt% glass fibers show that there are a greater number of dilational bands in specimens toughened with 100 wt% EPR-*g*-MA; this may explain why this

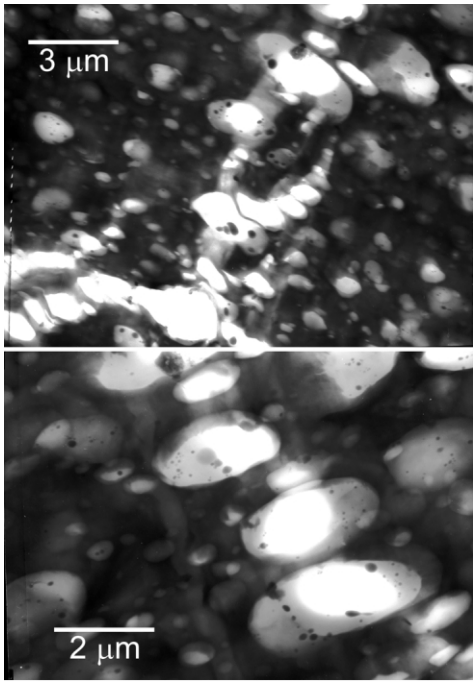

Fig. 21. TEM photomicrograph from a fractured Izod specimen of a blend toughened with 50/50 EPR-*g*-MA and reinforced with 15 wt% glass fibers showing a dilational band. The total rubber mass makes up 20 wt% of the polymer mass, excluding the glass fibers.

material has the highest fracture energy of the reinforced EPR/EPR-*g*-MA based materials. Unfortunately, microtoming samples that contain glass fibers produces sections that do not have large areas suitable for imaging. This difficulty in imaging large areas prevents a more quantitative analysis of the amount of deformation from these dilational bands.

Fig. 22 shows a TEM photomicrograph from a blend toughened with 100 wt% SEBS-*g*-MA and reinforced with 15 wt% glass fibers. The left-hand edge of this image is the Izod fracture surface. There is a small zone of shear yielding that extends less than 1 μm from the fracture surface. For all the glass fiber reinforced materials toughened with SEBS/SEBS-*g*-MA investigated, the size of this deformed zone

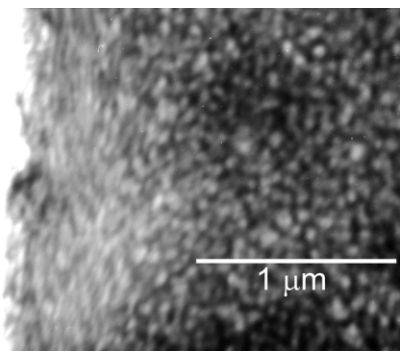

Fig. 22. TEM photomicrograph from a fractured Izod specimen of a blend toughened with 100 wt% SEBS-*g*-MA and reinforced with 15 wt% glass fibers. The left-hand side of the image shows the fracture surface. The total rubber mass makes up 20 wt% of the polymer mass, excluding the glass fibers.

was found to be constant regardless of the amount of maleation in the rubber phase, with the exception of the material containing no maleated rubber where this zone is smaller. Prior studies of these materials without glass fiber reinforcement showed that the size of this deformed zone increases from 8 μm when the rubber phase contains 100 wt% of SEBS-*g*-MA to 75 μm when the rubber phase contains 25 wt% of SEBS-*g*-MA [12]. Dilational bands like those seen in Figs. 20 and 21 were not seen in any materials made with SEBS/SEBS-*g*-MA. Since the size of the shear yielded zone is the same for all four materials containing SEBS-*g*-MA and there is no evidence of other deformational processes for these materials, it is reasonable that all four compositions should have similar fracture energies as shown in Figs. 13 and 16.

The shear yielded zone of the glass fiber reinforced SEBS/SEBS-*g*-MA toughened materials is much smaller than in materials made with EPR/EPR-*g*-MA. Fracture surfaces of the former materials display much less stress whitening than do the latter materials. In both cases, the size of the shear yielded zone is constant regardless of the rubber particle size; however, EPR/EPR-*g*-MA toughened materials have an additional toughening mechanism, i.e. the dilational bands. These dilational bands are more prevalent in the materials with smaller rubber particles leading to higher fracture energies for smaller rubber particles. The differences between the deformation mechanisms seen in glass fiber reinforced EPR/EPR-*g*-MA toughened blends and SEBS/SEBS-*g*-MA based materials can be understood based on the mechanical properties of the two elastomer systems. As mentioned above, rubber particle cavitation is not as prevalent when glass fibers are present. This lack of cavitation is exacerbated when SEBS-*g*-MA is used as a toughener because it has a higher shear modulus than EPR-*g*-MA [6,7]. This may explain the complete lack of cavitation and dilational bands when SEBS/SEBS-*g*-MA is used instead of EPR/EPR-*g*-MA. It is reasonable to assume that the differences in deformation processes between these two toughener systems accounts for the increased fracture energy when EPR/EPR-*g*-MA is used as the toughener.

7. Conclusions

The effects of rubber type and particle size on the mechanical properties of glass fiber reinforced nylon 6 were investigated; rubber particle size in the two systems could be easily varied by controlling the ratio of EPR to EPR-*g*-MA or SEBS to SEBS-*g*-MA in blends with nylon 6. When these blends are reinforced with 15 wt% glass fibers, the rubber particles are smaller than when no glass fibers are present. This decrease is approximately what is expected from the increase in apparent viscosity caused by the glass fibers.

The Izod impact strength of the glass fiber reinforced materials does not follow the same trend with rubber particle size as do the unreinforced materials. Unreinforced materials with the highest levels of toughness did not necessarily lead to the highest fracture energy when reinforced with 15 wt% glass fibers. An optimal SEBS/-SEBS-*g*-MA mixture leads to tougher blends with nylon 6 in the absence of glass fibers; however, EPR/EPR-*g*-MA based blends were tougher when reinforced with glass fibers. In terms of impact fracture parameters, nylon 6/SEBS-*g*-MA materials owe their high levels of toughness to high values of the dissipative energy density, u_d. On the other hand, the limiting specific fracture energy, u_0, is higher for EPR/EPR-*g*-MA based materials. The dissipative energy density is near zero for all materials containing 15 wt% glass fibers; thus, the SEBS/SEBS-*g*-MA based composites are not tougher than EPR/EPR-*g*-MA based composites. The limiting specific fracture energy, u_0, of the unreinforced materials appears to be a better predictor of relative fracture energies when glass fibers are added than is the Izod impact strength.

TEM observations of fractured specimens indicate that the damage zone size is much smaller in nylon 6/SEBS/-SEBS-*g*-MA materials containing 15 wt% glass fibers than in the glass fiber reinforced EPR/EPR-*g*-MA based materials. In addition, glass fiber reinforced nylon 6/EPR/EPR-*g*-MA blends develop zones like the dilational bands reported by Lazzeri and Bucknall [38] or croids described by Sue et al [39–41]; these are not seen in SEBS/SEBS-*g*-MA based materials. This feature is somewhat larger than traditional crazes, and appears to be due to polyamide ligament yielding between cavitated rubber particles. Glass fiber reinforced materials based on SEBS/SEBS-*g*-MA do not display this behavior or any evidence of rubber particle cavitation. The difference in deformed zone size and the lack of this craze-like deformation in SEBS/SEBS-*g*-MA materials that contain 15 wt% glass fibers seems to explain the lower fracture energies seen in glass fiber reinforced nylon 6/SES/SEBS-*g*-MA materials compared to reinforced EPR-*g*-MA based materials.

Acknowledgements

This research was supported in part by the Texas Advanced Technology program under Grant No. 003658-017. Allied Signal, Exxon, and Shell donated the polymers used in this research. Owens-Corning donated the glass fibers.

References

[1] Collyer AA, editor. Rubber toughened engineering plastics. London: Chapman & Hall; 1994.
[2] Paul DR, Newman S, editors. Polymer blends. New York: Academic Press Inc; 1978.

[3] Karger-Kocsis J. In: Paul DR, Bucknall CB, editors. Reinforced polymer blends. Polymer blends: formulation and performance, vol. 2. New York: Wiley; 2000. Chapter 31.
[4] Gaymans RJ. Toughened polyamides. In: Collyer AA, editor. Rubber toughened engineering plastics. London: Chapman & Hall; 1994. Chapter 7.
[5] Gaymans RJ, Oostenbrink AJ, van Bennekom ACM, Klaren JE. Fibre reinforced nylon–rubber blends. PRI Conference on Deformation and Fracture of Composites, Manchester; 1991. p. 23,21–23,25.
[6] Oshinski AJ, Keskkula H, Paul DR. Polymer 1992;33(2):268–83.
[7] Oshinski AJ, Keskkula H, Paul DR. Polymer 1996;37(22):4909–17.
[8] Oshinski AJ, Keskkula H, Paul DR. Polymer 1996;37(22):4919–28.
[9] Oshinski AJ, Keskkula H, Paul DR. J Appl Polym Sci 1996;61(4): 623–40.
[10] Bucknall CB, Karpodinis A, Zhang XC. J Mater Sci 1994;29: 3377–83.
[11] Bucknall CB, Heather PS, Lazzeri A. J Mater Sci 1989;16(6): 2255–61.
[12] Kayano Y, Keskkula H, Paul DR. Polymer 1997;38(3):1885–902.
[13] Kayano Y, Keskkula H, Paul DR. Polymer 1998;39(13):2835–45.
[14] Wu S. Polymer 1985;26(12):1855–63.
[15] Muratoglu OK, Argon AS, Cohens RE. Polymer 1995;36(5):921–30.
[16] Gaymans RJ. In: Paul DR, Bucknall CB, editors. Toughening of semicrystalline thermoplastics. Polymer blends, vol. 2. New York: Wiley; 2000. p. 177–224.
[17] Laura DM, Keskkula H, Barlow JW, Paul DR. Polymer 2002;43: 4673–87.
[18] Laura DM, Keskkula H, Barlow JW, Paul DR. Polymer 2001;42: 6161–72.
[19] Pressly TG, Keskkula H, Paul DR. Polymer 2000;42:3043–55.
[20] Kudva RA, Keskkula H, Paul DR. Polymer 2000;41(1):335–49.
[21] Mai Y-W, Wong S-C, Chen X-H. In: Paul DR, Bucknall CB, editors. Application of fracture mechanics for characterisation of toughness of polymer blends. Polymer blends: formulations and performance, vol. 2. New York: Wiley; 1999. Chapter 20.
[22] Wong S-C, Mai Y-W. Polym Engng Sci 1999;39(2):356–64.
[23] Wu J, Mai Y-W. Polym Engng Sci 1996;36(18):2275–88.
[24] Kim JK, Mai YW. Compos Sci Technol 1991;41:333.
[25] Mai Y-W. Polym Commun 1989;30:330–1.
[26] Mai Y-W, Cotterell B, Horlyck R, Vigna G. Polym Engng Sci 1987; 27:804.
[27] Mai YW, Cotterell B. Int J Fract 1986;32(2):105–25.
[28] Mai Y-W, Cotterell B. B Engng Fract Mech 1985;21:123.
[29] Mai YW. Engng Fract Mech 1985;21(1):123–8.
[30] Broberg KB. J Mech Phys Sol 1971;19(6):407–18.
[31] Broberg KB. J Mech Phys Sol 1975;23(3):215–37.
[32] Gonzales-Montiel A, Keskkula H, Paul DR. Polymer 1995;36(24): 4621–37.
[33] Plati E, Williams JG. Polym Engng Sci 1975;15(6):470–7.
[34] Okada O, Keskkula H, Paul DR. Polymer 2000;41:8061–74.
[35] Sue HJ, Yee AF. J Mater Sci 1991;26:3449–56.
[36] Wong S-C, Mai Y-W. Polymer 2000;41:5471–83.
[37] Bucknall CB. Toughened plastics. London: Applied Science Publishers Ltd; 1977.
[38] Lazzeri A, Bucknall CB. Polymer 1995;36(15):2895–902.
[39] Sue HJ. J Mater Sci 1992;27:3098–107.
[40] Sue H-J, Bertram JL, Garcia-Meitin EI, Puckett PM. J Polym Sci, Part B: Polym Phys 1995;33(14):2003–17.
[41] Sue H-J, Garcia-Meitin EI, Orchard NA. J Polym Sci, Part B: Polym Phys 1993;31(5):595–608.